# Regional Weather Patterns during Anomalous Air–Sea Fluxes at the Kuroshio Extension Observatory (KEO)*

NICHOLAS A. BOND

*Joint Institute for the Study of the Atmosphere and Ocean, University of Washington, Seattle, Washington*

MEGHAN F. CRONIN

*National Oceanic and Atmospheric Administration/Pacific Marine Environmental Laboratory, Seattle, Washington*

(Manuscript received 1 December 2006, in final form 6 September 2007)

ABSTRACT

The weather patterns during periods of anomalous surface fluxes in the Kuroshio recirculation gyre of the western North Pacific are documented. Separate analyses are carried out for the cold season (October–March) when the net surface heat flux is controlled by the combination of the turbulent sensible and latent heat fluxes ($Q_{\text{turb}}$), and for the warm season (May–August) when the net heating is dominated by the net radiative fluxes ($Q_{\text{rad}}$). For analysis of high-frequency (daily to weekly) variations in the fluxes, direct measurements from the Kuroshio Extension Observatory (KEO) for the period June 2004–November 2005 are used to specify flux events. For analysis of interannual variations, these events are selected using NCEP–NCAR reanalysis estimates for $Q_{\text{turb}}$ in the cold season, and International Comprehensive Ocean–Atmosphere Data Set (ICOADS) data for cloud fraction, as a proxy for $Q_{\text{rad}}$, in the warm season.

During the cold season, episodic high-frequency flux events are associated with significant anomalies in the east–west sea level pressure gradients, and hence meridional winds and lower-tropospheric air temperature, reflecting the dominance of the atmospheric forcing of the flux variability. On the other hand, interannual variations in $Q_{\text{turb}}$ are associated with relatively weak atmospheric circulation anomalies, implying a relatively important role for the ocean. During the warm season, high-frequency fluctuations in the net surface fluxes occur due to a mix of anomalies in $Q_{\text{turb}}$ and $Q_{\text{rad}}$. Enhanced cloudiness in the vicinity of KEO, and hence reduced $Q_{\text{rad}}$, tends to occur in association with weak cyclonic disturbances of extratropical origin. A regional atmospheric circulation favoring these types of events also was found for warm seasons that were cloudier on the whole. Results suggest that the ocean's influence on air–sea fluxes at KEO is manifested mostly on interannual time scales during the cold season.

## 1. Introduction

Air–sea interactions are particularly strong in the region of the recirculation gyre south of the Kuroshio Extension in the western North Pacific Ocean. Frequent outbreaks of cold, dry air of continental origin over the relatively warm ocean during winter results in this region experiencing the largest mean surface heat fluxes of the entire Pacific basin (Josey et al. 1998). These heat fluxes are an aspect of the global heat cycle and affect how the net poleward heat transport is partitioned between the atmosphere and ocean (Trenberth and Caron 2001). In the tropics the poleward heat transport is dominated by the ocean, while north of the Kuroshio Extension the meridional heat transport is dominated by the atmosphere. The regional air–sea heat fluxes also have specific impacts on both the ocean, notably in terms of their role in forming subtropical mode water (STMW), and on the atmosphere, with the latter impacts felt far downstream. For example, the SST of the region, presumably as communicated through the regional fluxes, was shown recently to be a significant predictor of wintertime air temperature in the northern United States (Quan et al. 2006).

* National Oceanic and Atmospheric Administration/Pacific Marine Environmental Laboratory Contribution Number 3028.

*Corresponding author address:* Dr. Nicholas A. Bond, NOAA/PMEL, 7600 Sand Point Way NE, Seattle, WA 98115.
E-mail: nicholas.bond@noaa.gov

DOI: 10.1175/2007JCLI1797.1

The heat fluxes at the air–sea interface reflect the disequilibrium between the atmosphere and ocean; so, in principle, either medium represents a source of variability in the fluxes. The degree to which the atmosphere versus the ocean is responsible for this variability, as a function of time scale, has not been fully established.

The atmosphere controls the high-frequency variability in the regional heat fluxes during winter. Depending on the regional atmospheric circulation (i.e., the synoptic-scale weather pattern), the recirculation gyre experiences a wide range of air masses from warm, maritime air of lower-latitude origin to the aforementioned cold, continental air. These cold air outbreaks off the coast of East Asia were targeted by the Air Mass Transformation Experiment (AMTEX) in an observational study of atmospheric boundary layer (ABL) modification during periods of intense surface heating and moistening (Lenschow and Agee 1976). While the weather pattern for this situation is well appreciated in a general sense, little attention has been paid to the opposite situation, that is, to periods of anomalous downward surface heat fluxes. Even less is known about the weather patterns associated with anomalous surface heat fluxes in the summer. It might be expected that the net heat fluxes of the region are dominated by the surface sensible and latent heat fluxes in winter, and by the radiative heat fluxes in summer, and it is therefore reasonable to suppose that different kinds of weather patterns are responsible for flux anomalies at different times of the year. Comparison of the winter with the summer weather patterns driving short-term flux variability represents one of the two primary objectives of this paper.

On yearly and longer time scales, the temperature fluctuations for the lower atmosphere and upper ocean are more comparable, and the latter is more apt to play a significant role in determining heat flux variability. In particular, Tanimoto et al. (2003) show that the SST anomalies are responsible for much of the observed variability in the surface fluxes on decadal time scales for the region east and south of Japan. Additional evidence in support of this idea is provided by the observational and modeling studies of Kelly (2004) and Seager et al. (2001), respectively. The second objective of this paper is to apply the results from the analysis of the high-frequency variability to further investigate the importance of oceanic conditions on lower-frequency flux variability at the recirculation gyre. This is accomplished by comparing the weather patterns characteristic of short time-scale fluctuations in the fluxes, for which the atmospheric variability dominates that for the ocean, with the weather patterns characteristic of seasonal mean fluctuations in the fluxes, for which both atmospheric and oceanic variability are potentially important. In other words, the extent to which these patterns match helps indicate the degree to which the atmosphere controls the variability in the fluxes on longer time scales.

Our analysis of the fluxes on short time scales is made feasible through measurements from a surface meteorological buoy, the Kuroshio Extension Observatory (KEO), located in the recirculation gyre just south of the Kuroshio Extension jet. As such, this location is also just south of a maximum in the average wintertime (December–February) net heat flux from the ocean to atmosphere (e.g., Qiu et al. 2004). The KEO platform is used to specify daily averages of the individual elements of the air–sea fluxes, including surface sensible and latent heat fluxes (hereafter as combined termed $Q_{\text{turb}}$), net longwave and shortwave radiative fluxes (hereafter as combined termed $Q_{\text{rad}}$), and surface wind stresses. These in situ measurements are valuable because, as shown by Moore and Renfrew (2002) and Cronin et al. (2006b), surface heat fluxes are not necessarily well diagnosed by reanalysis products such as the National Centers for Environmental Prediction–National Center for Atmospheric Research (NCEP–NCAR) reanalysis (NNR) (Kalnay et al. 1996; Kistler et al. 2001). Of particular relevance to the present study is the analysis by Kubota et al. (2008), which consists of detailed comparisons of the surface fluxes from KEO with their counterparts from NNR. The radiative fluxes are especially prone to error due to the difficulties that reanalyses in general (not just the NNR) have in characterizing clouds and their effects (e.g., Cronin et al. 2006a,b). On the other hand, NNR and other reanalyses provide reliable descriptions of regional atmospheric circulations (Moore and Renfrew 2002; Renfrew et al. 2002; Ladd and Bond 2002). These products therefore are suitable for depicting the weather patterns associated with periods of anomalous surface fluxes, even if they might include errors in the magnitudes of the fluxes themselves.

The analysis is carried out separately for a cold and a warm season, which are defined in terms of the nature of the atmospheric forcing in the vicinity of KEO. Daily values of the net surface heat fluxes from KEO relative to a low-pass filtered mean are used to specify the periods of anomalous ocean heat loss and gain at the KEO site. We consider the separate contributions of $Q_{\text{turb}}$ and $Q_{\text{rad}}$ to the net surface heat fluxes during these periods and compare them with their counterparts from NNR to determine the capability of the latter for characterizing significant anomalies in forcing. Composite sea level pressure anomaly (SLPA) and 850-hPa air temperature maps for the periods of anomalous

forcing in each season are used to describe regional weather conditions. The record for this portion of the analysis is the first two deployments of KEO from June 2004 to November 2005.

We build upon our analysis of the high-frequency variations in the surface fluxes at KEO to provide new information on the relationships between the atmospheric circulation and interannual variations in the fluxes of the region. Determination of the weather patterns associated with longer-term variations in the fluxes requires specification of the years for which the surface fluxes were significantly anomalous; it appears that the multidecadal record of NNR, supplemented by cloud information from International Comprehensive Ocean–Atmosphere Data Set (ICOADS), is adequate for this purpose. As with the KEO time period, the cold and warm seasons are considered separately.

The paper is organized as follows. A brief description of the data and methods is provided in the next section. An overview of the fluxes observed at KEO is also presented, with an emphasis on their seasonal variation. The bulk of the paper is represented by sections 3 and 4. The former features depiction of the weather patterns with short-term variations in the fluxes as a function of season and includes a brief treatment of the weather associated with episodes of wind mixing. Section 4 focuses on the interannual variations in air–sea interactions at KEO. The last section consists of concluding remarks.

## 2. Data and methods

Detailed descriptions of the KEO buoy and its datasets are provided in Kubota et al. (2008), and on the following Web site: http://pmel.noaa.gov/keo/. The KEO buoy is located at 32.4°N, 144.6°E in the Kuroshio Extension recirculation gyre and carries a full suite of meteorological sensors to monitor conditions at the air–sea interface. The analysis for this paper uses the high-resolution (10 minute to hourly) KEO data converted into daily averages for the period of the first two deployments (17 June 2004 to 4 November 2005). Cronin et al. (2006b) carried out an error analysis for buoys with similar suites of instruments in the eastern tropical Pacific, considering sensor errors and mesoscale variability, which is especially important in terms of the representativeness of point measurements of downward solar radiation. They found errors in the daily average heat fluxes of roughly 10 W $m^{-2}$ for $Q_{turb}$ and 10 W $m^{-2}$ for $Q_{rad}$. An error analysis of the fluxes from KEO is provided by Kubota et al. (2008). Kubota et al. (2008) also show that systematic differences between the KEO and NNR fluxes are reduced if the latter are recalculated using basic-state variables and the Tropical Ocean and Global Atmosphere Coupled Ocean–Atmosphere Response Experiment (TOGA COARE) flux algorithm (Fairall et al. 2003). For the present study, the unadjusted values of these components seem to be sufficient for identifying the years with significant seasonal mean anomalies in $Q_{turb}$.

The basic time series of the fluxes shown in Fig. 1 represent a logical basis for defining the two primary seasons at KEO. The cold season is considered to be the period October through March. We note that this period at KEO features deepening and cooling of the oceanic mixed layer (not shown), and generally large values of $Q_{turb}$ (positive values signify upward heat fluxes from the ocean to atmosphere), with considerable day-to-day variability, and consistently small values of $Q_{rad}$ (positive values here signify downward fluxes heating the ocean). The warm season is defined as May through August. The mixed layer during this time of year is shallow and warming (not shown) and the net heat fluxes are systematically downward due to the predominance of $Q_{rad}$ (principally the shortwave component) over $Q_{turb}$. The average net heating during the transition months of April and September is minimal and neither $Q_{turb}$ nor $Q_{rad}$ dominates the variability; for simplicity we exclude those months in the following analysis. Summary statistics for the cold and warm seasons are listed in Table 1.

There is good correspondence between the daily variations in KEO $Q_{turb}$ and those in NNR $Q_{turb}$ during the cold season (Table 1), which suggests that NNR represents a reliable source of information for multiyear, retrospective analysis of $Q_{turb}$ in the vicinity of KEO. Qiu et al. (2004) also compared heat fluxes and wind stresses from NNR with direct measures from a moored buoy, in their case located southwest of KEO at 29°N, 135°E. Their results are mostly consistent with the results reported by Kubota et al. (2008) and summarized here. Specifically, as shown by Qiu et al. (2004), while NNR systematically overestimates $Q_{turb}$, it does correctly identify the significant flux events. NNR diagnoses the variability in the radiative heat fluxes with less fidelity, especially in the warm season when the effects of clouds are larger.

### *a. Subseasonal analysis*

The periods of anomalous heat fluxes are defined as those days for which the daily values of the net heat fluxes (i.e., the combination of $Q_{turb}$ and $Q_{rad}$) differ from the background by greater than one standard deviation. The background values were computed using a triangular filter (a 15-day running mean applied twice) on the KEO daily values, with extrapolation to the ends

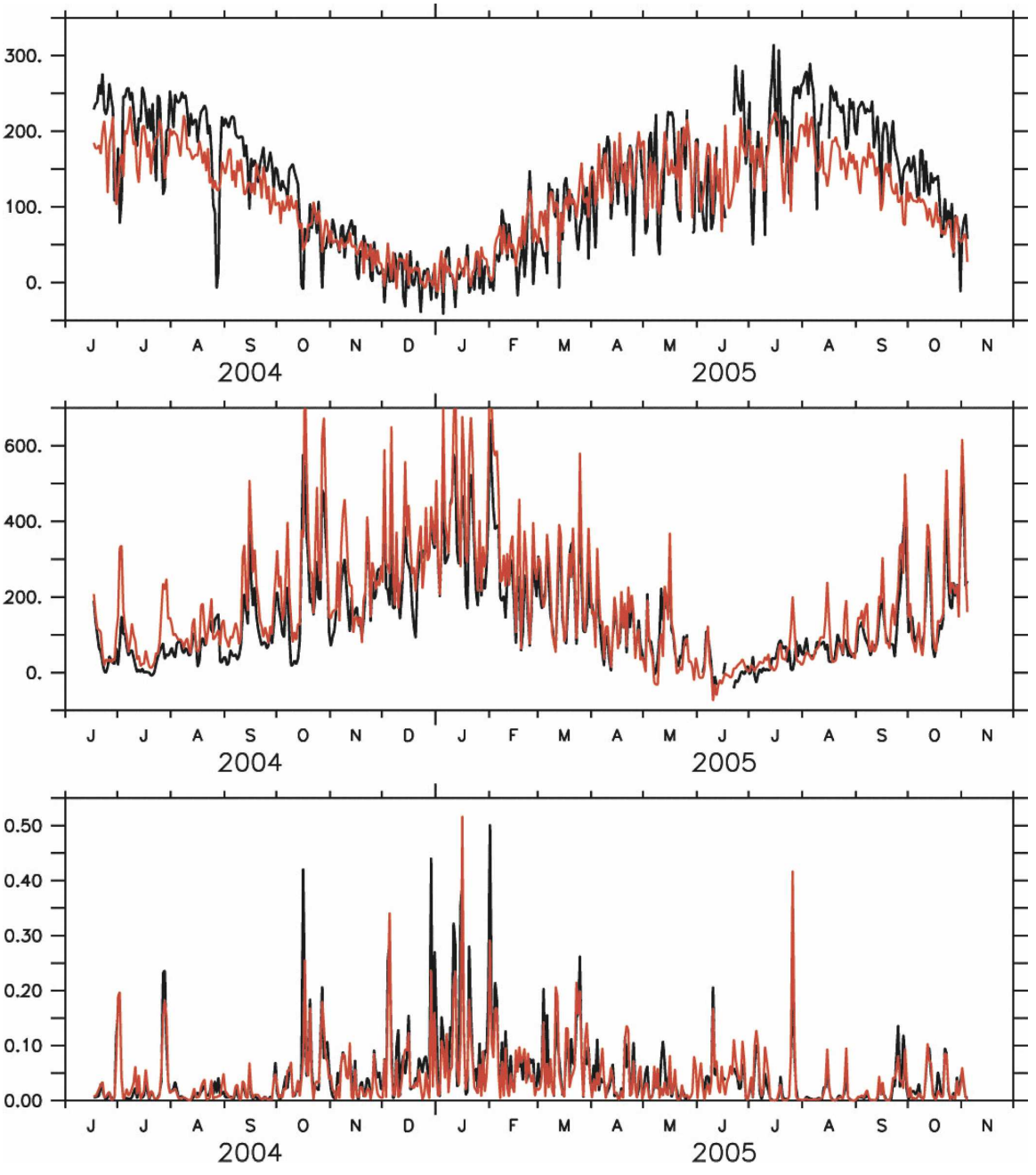


FIG. 1. Time series of daily average (top) $Q_{rad}$ (W m$^{-2}$), (middle) $Q_{turb}$ (W m$^{-2}$), and (bottom) atmospheric friction velocity cubed ($U_*^3$) (m$^3$ s$^{-3}$), where $U_* = (\tau/\rho)^{1/2}$, from KEO (black) and from NNR (red). Positive values of $Q_{rad}$ ($Q_{turb}$) signify downward (upward) fluxes and hence heating (cooling) of the ocean.

of the dataset and linear interpolation for a few brief interruptions in the middle of the dataset. The difference between the raw and filtered time series of net heat fluxes effectively represents the fluctuations on time scales of less than 2–3 weeks. The days identified using the method described above are grouped seasonally. The sets of anomalous cooling and heating events comprise 33 and 30 days, respectively, during the cold season and 25 and 19 days, respectively, during the warm season. The weather patterns for the periods of anomalous heating and cooling within each season are portrayed in terms of composite SLPA maps for the days with anomalous surface heating and cooling and a map portraying the composite difference in 850-hPa air

TABLE 1. Surface heat fluxes (means and standard deviations; W $m^{-2}$) from the KEO and the NNR, and correlation coefficients ($r$) between daily values from KEO and NNR.

| Season | KEO $Q_{rad}$ | NNR $Q_{rad}$ | $r$ | KEO $Q_{turb}$ | NNR $Q_{turb}$ | $r$ |
|---|---|---|---|---|---|---|
| Cold | 57 ± 52 | 58 ± 38 | 0.82 | −240 ± 126 | −298 ± 161 | 0.92 |
| Warm | 193 ± 64 | 165 ± 34 | 0.63 | −53 ± 50 | −68 ± 70 | 0.66 |

temperature difference map between the two flux regimes. The baselines for computing these anomalies were determined in the same manner as for the fluxes. This was done for the sake of consistency in that the fluctuations in both the fluxes and the regional weather patterns were considered relative to the period of the KEO deployment. The regions of statistically significant perturbations are indicated on the SLPA maps. Other meteorological fields were examined: we feel that the SLPA and 850-hPa maps depict the regional atmospheric circulation anomalies in a sufficiently complete manner.

The distributions of SLP and 850-hPa air temperature from NNR are considered reliable for the present purposes. Both are so-called prognostic variables (Kalnay et al. 1996) that are constrained by observations, which, at least for SLP, are relatively abundant. As mentioned earlier, previous work (e.g., Renfrew et al. 2002) has shown that reanalysis products are able to diagnose basic meteorological fields, especially SLP, with good fidelity. These results are supported by tests carried out for the present study. For example, a correlation coefficient of ~0.9 was found between the daily average meridional wind measured at KEO and its counterpart from NNR, signifying that NNR represents the day-to-day distributions of SLP accurately.

### b. Interannual analysis

The analysis of the interannual variations in heat fluxes in the vicinity of KEO is based on NNR, supplemented by ICOADS. The NNR dataset was used to compute mean values of $Q_{turb}$ at KEO for the cold seasons, defined as October through March, for the years from 1949 to 2005. These values are for the grid point nearest to KEO at 31.4°N, 144.4°E; very similar results were obtained from averages for a 5° × 5° box at KEO. The period of October through March represents the time of year for which $Q_{turb}$ dominates the net surface heat flux (Fig. 1); similar results were found in tests using a shorter winter season. The weather patterns accompanying seasonal flux anomalies were determined following the procedure used in the analysis of the high-frequency fluctuations from KEO. Years for which the fluxes differed from the mean by greater than one standard deviation were assembled; the corresponding composite SLPA, 850-hPa air temperature, and SST data from NNR are used to represent the seasonal mean atmospheric and oceanic conditions during anomalous cooling and heating of the ocean due to $Q_{turb}$. In addition, the associations between the seasonal mean $Q_{turb}$ and local basic-state parameters (such as surface air temperature, 850-hPa wind, and sea surface temperature) and commonly used indices for characterizing the climate are assessed using a simple linear correlation analysis.

A similar analysis was carried out on the interannual variability during the warm season, with some distinctions. First of all, the warm season here is defined as the 4-month period of May through August because it represents the time of year when the shortwave component of the radiative fluxes dominates the net surface heating at KEO. Since the radiative fluxes are not handled well by NNR (Table 1), as also found by Kubota et al. (2008), we used cloud coverage observations from ICOADS as a proxy for the solar component. We inspected the cloud data from ICOADS for the KEO region for each month, and it appears that reasonable data extends back to 1954.

We have compared seasonal averages in cloud cover from ICOADS with those in surface downward shortwave radiation from the International Satellite Cloud Climatology Project (ISSCP). The correlation coefficient between these two records at the KEO site over the 19 years of overlap in the records is significantly negative ($r \sim -0.55$) based on a Student's $t$ test. On the other hand, the interannual variations in cloud coverage from ICOADS and downward shortwave radiation from NNR are actually positively correlated ($r \sim 0.33$). We have no explanation for this result. We do not use ISSCP in our selection of anomalous warm seasons because this information is available for less than one-half as long as the cloud coverage data from ICOADS and, hence, limited in terms of degrees of freedom.

We note that a series of papers by J. Norris and collaborators (e.g., Norris et al. 1998; Norris 2000) also incorporate surface marine observations (i.e., the same basic source as for ICOADS) to characterize spatial and temporal patterns in summertime clouds. As with the cold season analysis that used $Q_{turb}$ as a criterion, years with significant cloud coverage anomalies were

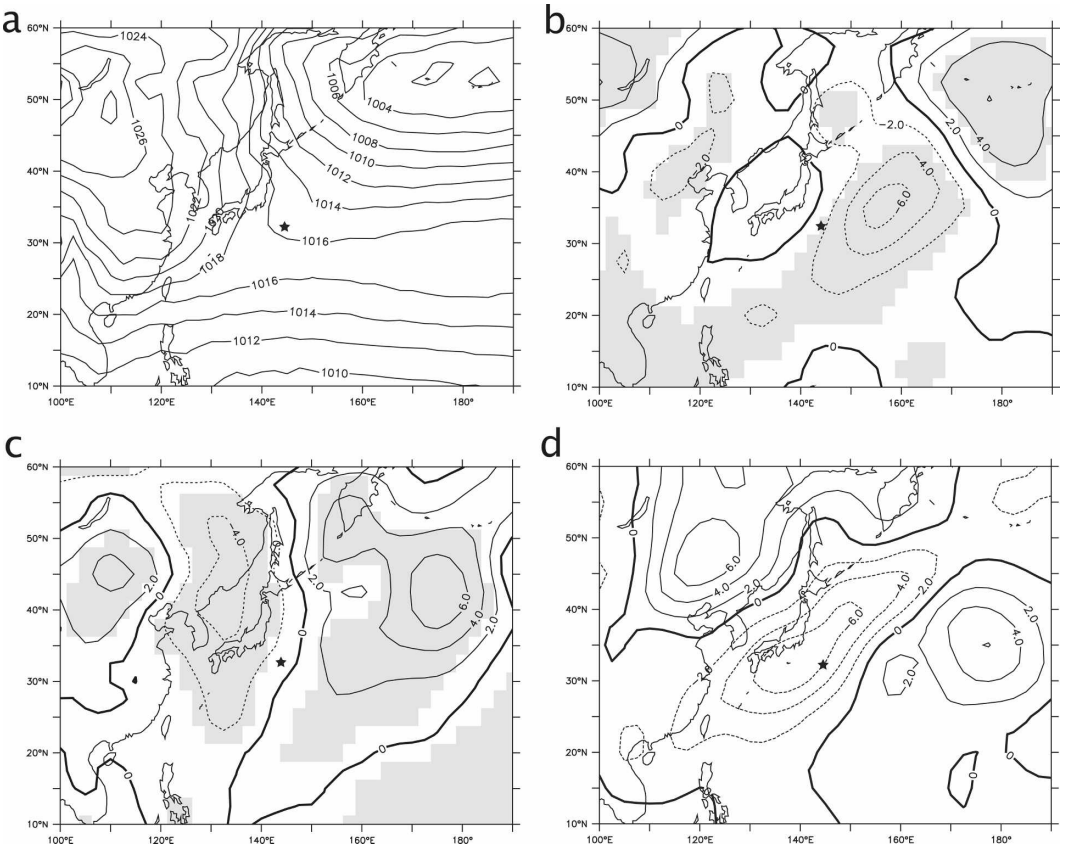


FIG. 2. Cold season (a) mean SLP (contour interval 2 mb), (b) composite SLPA distribution (contour interval 2 mb) during periods of anomalous heat loss, (c) composite SLPA distribution (contour interval 2 mb) during periods of anomalous heat gain, and (d) composite 850-hPa air temperature difference (contour interval 1°C) between periods of anomalous heat loss and anomalous heat gain. Shading in (b) and (c) indicates where SLPA signals are statistically significant, based on the standard deviation in daily SLP during period of KEO deployment. The star indicates location of the KEO.

grouped for the purpose of determining the regional atmospheric circulations and SST distributions characteristic of relatively cloudy and clear warm seasons. We recognize that our results based on the ICOADS cloud observations are tentative, owing to errors involving data quality and scarcity, and since fractional cloud coverage represents an indirect and inexact measure of the solar irradiance.

## 3. Weather patterns associated with episodic forcing

### *a. Anomalous heat fluxes at KEO*

The weather patterns associated with major episodic forcing events in the cold and warm seasons during the KEO deployment are shown here. The mean SLP distribution for the cold season (Fig. 2a), defined as October through March, illustrates that KEO is in a location of mean northwesterly winds driven by the SLP gradient between high pressure centered over Mongolia and low pressure centered near the western Aleutian Islands. The periods of analysis for this study, 1 October 2005 through 31 March 2005 and 1 October 2005 through 4 November 2005, included a weak low-level southerly wind anomaly ($\sim$1 m s$^{-1}$) and a positive air temperature anomaly ($\sim$0.5°C) relative to their long-term climatological means. The period of record at KEO reflects typical cold season conditions, at least in the mean sense.

Periods of enhanced net heat loss (>130 W m$^{-2}$ above normal) during the cold season tend to occur in conditions of anomalous troughing to the northeast of KEO and weaker high pressure west of KEO and, hence, relatively strong northerly flow (Fig. 2b). In the majority of cases, this situation occurred when KEO was in the southwest sector of cyclonic disturbances propagating from the coast into the west-central North

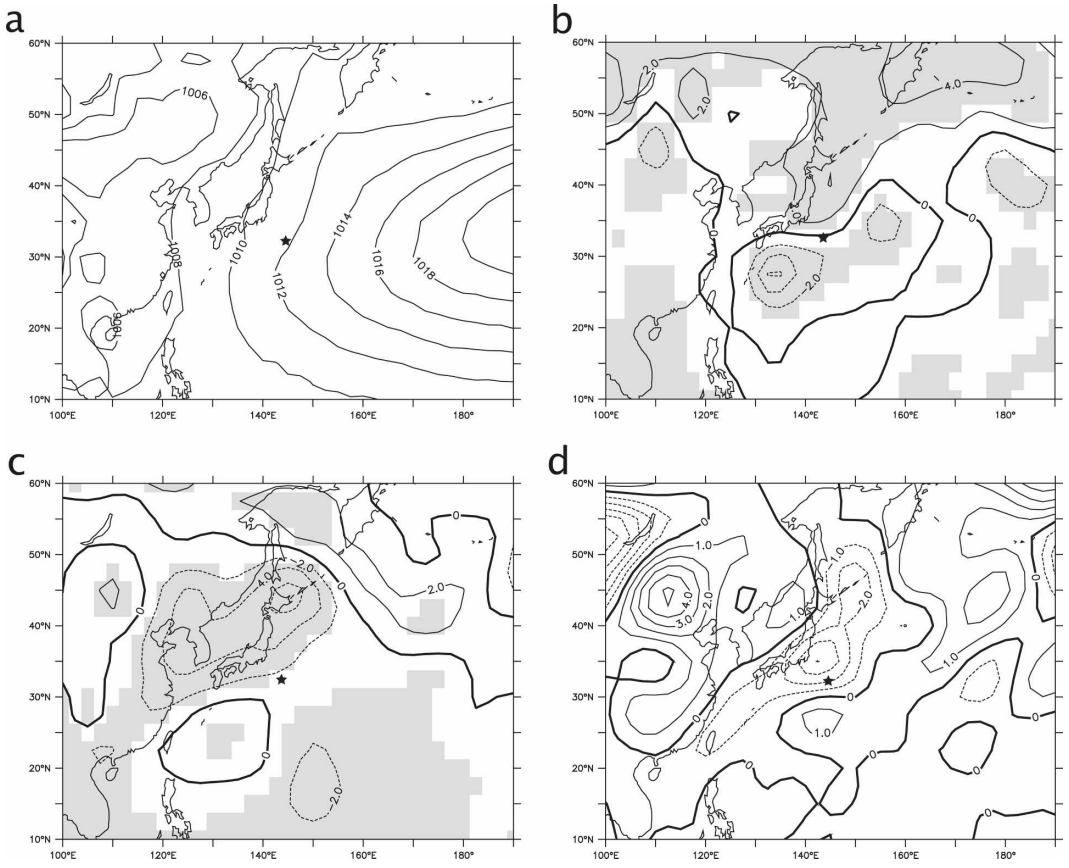


FIG. 3. As in Fig. 2 but for the warm season.

Pacific. As might be expected, this situation leads to much above normal heat losses due to the twin effects of relatively strong winds and larger thermodynamic disequilibrium between the atmosphere and ocean than normal and hence large upward $Q_{\text{turb}}$; $Q_{\text{rad}}$ plays a minimal role in determining the net surface heat flux anomalies. During these events, the mean error in the net heat loss by NNR is 88 W $m^{-2}$, or about 50% greater than that for the cold season as a whole, but there is good agreement between KEO and NNR in terms of identifying events.

The SLPA pattern during episodes of anomalous heat gain (Fig. 2c) is close to opposite that during episodes of anomalous heat loss. In these situations, for which the heat loss is just significantly less than average, there tends to be anomalously low pressure just west of KEO and, hence, anomalous southerly flow of relatively warm and moist air out of the subtropics.

The 850-hPa temperature difference map (Fig. 2d) shows that episodes of large (small) upward heat fluxes in winter are associated with periods of markedly cold (warm) lower-tropospheric temperatures. In general, the day-to-day variations in SST are less than one-tenth as large as those in 850-hPa temperature and the former have a correlation of essentially zero with the day-to-day variations in the net heat fluxes.

The mean SLP distribution for the warm season (Fig. 3a) illustrates that the KEO location experiences mean southerly flow due to continental low pressure to its west and the North Pacific high to its east. The periods of analysis for this study, 17 June 2004 through 31 August 2004 and 1 May 2005 through 31 August 2005, were characterized by low-level flow anomalies of ~2 m $s^{-1}$ from the east-southeast and west, respectively. In combination, the two periods appear to be fairly representative of typical warm season conditions for the location of KEO.

The one standard deviation threshold for anomalous cooling/heating during the warm season is 64 W $m^{-2}$ or about one-half that during the cold season. Anomalous cooling during the warm season coincided with lower than normal SLP southeast of KEO and higher than normal SLP from the Sea of Okhotsk into the western Bering Sea (Fig. 3b). This pattern resembles the synoptic situation found by Ninomiya and Mizuno (1985) for summertime cold spells in northeastern Japan. In-

spection of the individual events constituting the composite indicates a preponderance of cyclones of tropical origin passing to the southwest of KEO in 2004 and weaker cyclonic disturbances of extratropical origin near KEO in 2005. The former events tend to include both low $Q_{rad}$ (enhanced cloudiness) and high $Q_{turb}$ (due to relatively strong winds), while the latter events tend to include enhanced cloudiness but significant $Q_{turb}$ anomalies only occasionally. Discrepancies in the net heating between KEO and the NNR were modest ($\sim$23 W m$^{-2}$), but NNR indicated an excessive $Q_{rad}$ of $\sim$41 W m$^{-2}$ compensated in part by an overestimate of outgoing $Q_{turb}$. Anomalous heating during the warm season (Fig. 3c) was associated with negative SLPA to the northwest of KEO centered over the Sea of Japan and weak positive SLPA southwest of KEO, resulting in anomalous west-southwesterly flow. The anomalous heating in these situations can be attributed to both less cloud cover and reduced $Q_{turb}$. These situations were accompanied by a mean net heating from NNR that was 93 W m$^{-2}$ less than that from KEO, mostly due to underestimation of $Q_{rad}$.

The 850-hPa temperature difference pattern for the warm season (Fig. 3d) features a southwest–northeast oriented band of negative values from off the coast of China to east of Japan. The magnitude of this temperature difference at KEO is approximately $-2$°C, or about one-third of its counterpart for the cold season. With respect to the mean low-level flow, the peak negative values are downstream of KEO during the warm season and upstream of KEO during the cold season. This represents another piece of evidence that a different set of mechanisms control the variability in the net surface heat fluxes in the two seasons.

We feel that the results presented above represent reliable descriptions of the weather patterns associated with short-term net heat flux anomalies, even though they are based on a relatively short dataset. The SLPA patterns for anomalous cooling are close to opposite to those for anomalous warming (to a lesser extent in the warm season), especially in the immediate vicinity of KEO. In general, KEO is near a node in these SLPA patterns but in a region of significant anomalous pressure gradient, implying robust signatures in the winds. Moreover, the SLPA and 850-hPa temperature fields for the individual events within the composites (not shown), while including case-to-case variations, tend to resemble one another. Therefore, a few extreme cases do not dominate the composites of Figs. 2 and 3.

### *b. Wind mixing of the upper ocean at KEO*

Wind mixing events at KEO are highly episodic, as indicated by the time series for atmospheric $U_*^3$ from KEO and NNR (Fig. 1). The purpose of the present section is to explore how the weather patterns associated with strong winds vary seasonally.

TABLE 2. Mean wind mixing (m$^3$ s$^{-3}$) from KEO and the NNR and correlation coefficients between their daily values.

| Season | KEO $U_*^3$ | NNR $U_*^3$ | $r$ |
|---|---|---|---|
| Cold | 0.071 | 0.057 | 0.83 |
| Warm | 0.027 | 0.029 | 0.87 |

The seasonal mean values of $U_*^3$ from KEO and NNR (Table 2) closely match for the warm season, but NNR underestimates the mean $U_*^3$ for the cold season. Much of this error is liable to be associated with the NNR's inability to characterize the mesoscale variability accompanying storms and, hence, short bursts of strong winds impacting daily averages. Owing to the cubic nature of the wind mixing, these bursts represent a disproportionate fraction of the seasonal average. The high correlation coefficients between the daily variations in $U_*^3$ from the KEO and NNR supports our contention made earlier that the NNR characterizes the regional atmospheric circulation reasonably well. This result is consistent with a previous evaluation of how winds from NNR compare with directly measured winds at buoys in the Bering Sea and North Pacific (Ladd and Bond 2002).

Composite SLP anomaly maps were produced for the wind events during each season, as defined by those days for which $U_*^3$ exceeded its seasonal mean value by one standard deviation. The SLPA pattern for windy conditions in the cold season features a negative center just north of KEO, which generally occurs in association with a southward displaced storm track (Fig. 4). Windy conditions in the warm season (Fig. 5) tend to be associated with anomalously low pressure immediately to the west of KEO, which serves to enhance the prevailing southerly winds of the season. Two of the events included in the composite occurred when tropical cyclones were near KEO (Ting-Ting in late June 2004 and Namtheun in late July 2004); removal of these cases does not change the character of the SLPA pattern in the vicinity of KEO (not shown). The results for the period of the KEO deployment therefore appear to be representative.

## 4. Interannual variations in air–sea interactions

The objective here is to examine the extent to which year-to-year fluctuations in the surface heat fluxes are associated with the regional weather/atmospheric conditions versus the state of the underlying ocean. While

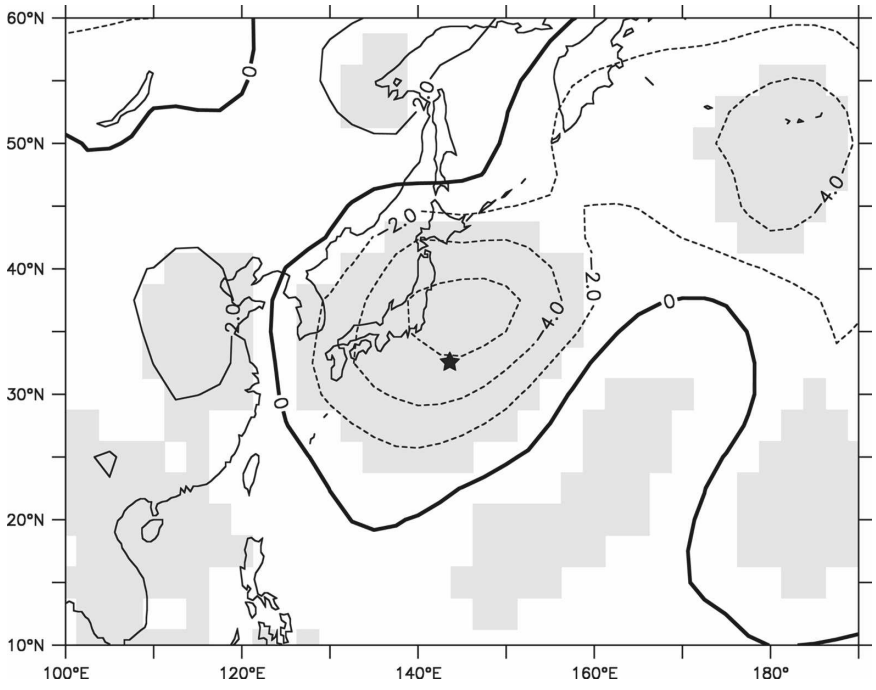


FIG. 4. Composite SLPA distribution (contour interval 2 mb) during periods of anomalously strong wind mixing in the cold season. Shading indicates regions of statistically significant SLPA signal. The star indicates location of the KEO.

upper-ocean thermal variations tend to be smaller than those for the atmosphere, they also tend to persist longer, and it can be reasonably supposed that the ocean has a larger influence on the fluxes on longer time scales. Moreover, the KEO region features relatively large SST gradients and vigorous eddy activity. All of this is consistent with previous studies asserting that the atmosphere is relatively sensitive to oceanic

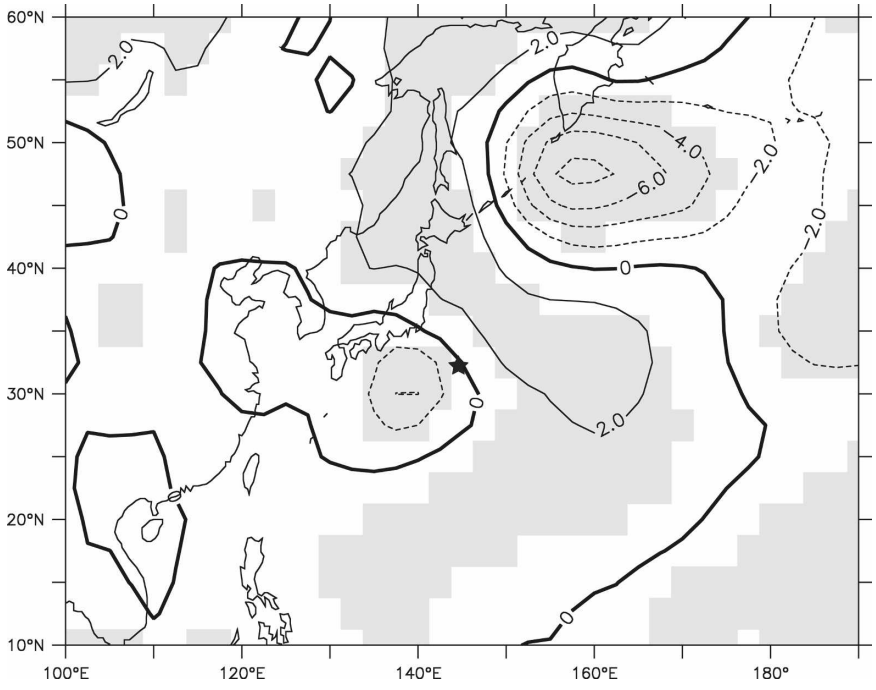


FIG. 5. As in Fig. 4 but for the warm season.

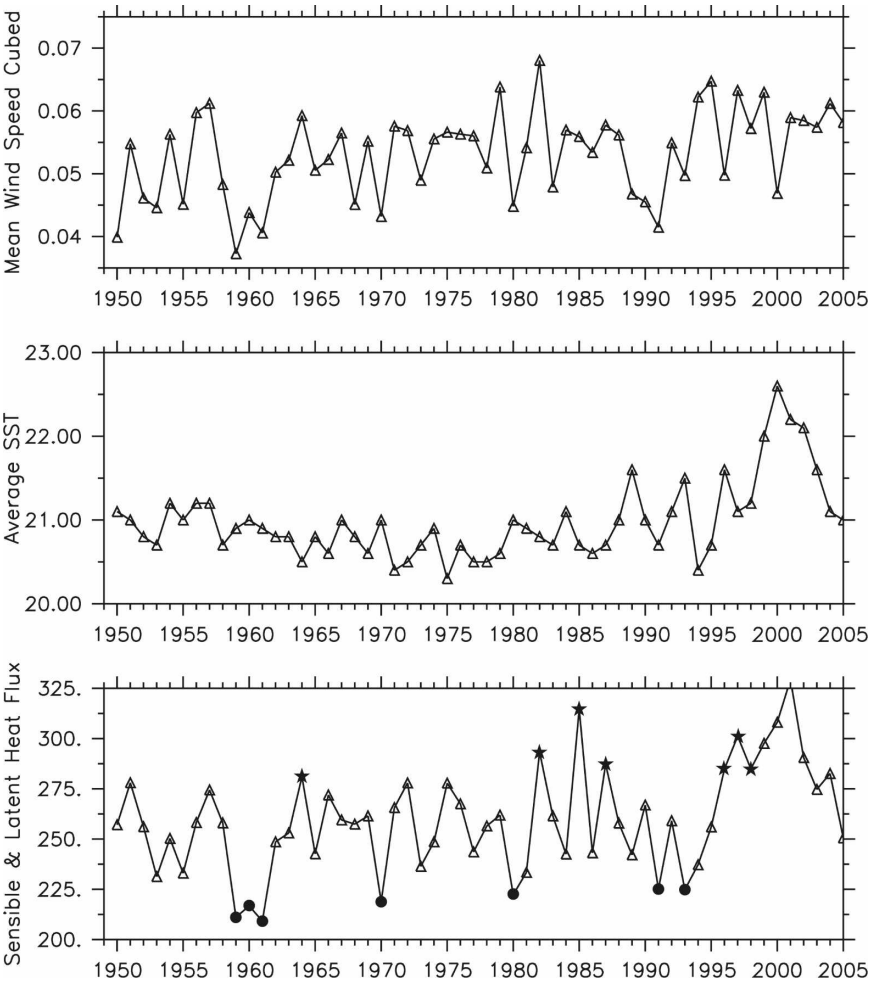


FIG. 6. Mean cold season (top) $U_*^3$ ($m^3 s^{-3}$), (middle) SST (°C), and (bottom) $Q_{turb}$ (W $m^{-2}$) from NNR at KEO. The years included in the high and low $Q_{turb}$ composites are indicated with stars and solid circles, respectively.

variability in the KEO region (Kelly 2004, among others).

As a means of pursuing this issue, we take advantage of the five-decade-long record from the NNR. We consider just $Q_{turb}$ during the cold season because, as shown earlier, the radiative fluxes are less important and are not as reliably diagnosed by NNR. The time series of seasonal mean $Q_{turb}$, $U_*^3$, and SST for the period of record are plotted in Fig. 6. Notable fluctuations in $Q_{turb}$ include low values from 1959 to 1961, which were accompanied by relatively weak winds, and the period near the turn of century, which featured very warm SSTs. These positive SST anomalies were not a local effect due to changes in the position of the Kuroshio Extension. Instead, they occurred over a large region in the western North Pacific (Fig. 7). During this period, the SST distribution for the North Pacific as a whole can be attributed in large part to a strong expression in the second leading mode of wintertime SST variability in the North Pacific (Bond et al. 2003). The SLPA distribution for this same period features relatively low pressure over East Asia and high pressure east of the date line (Minobe 2002), implying anomalous low-level winds from the south over the western North Pacific.

Regardless of the cause(s) of this anomalously warm water, previous studies (notably Tomita and Kubota 2005) have demonstrated that the anomalously high $Q_{turb}$ in this period can be largely attributed to the concomitant anomalies in SST. Because this period appears to be unusual, we believe it makes sense to exclude it for the purpose of determining the typical weather and SST patterns that are associated with seasonal mean anomalies in $Q_{turb}$ in the vicinity of KEO. Hence, for this purpose, we have focused our attention on the cold seasons from 1950 to 1998.

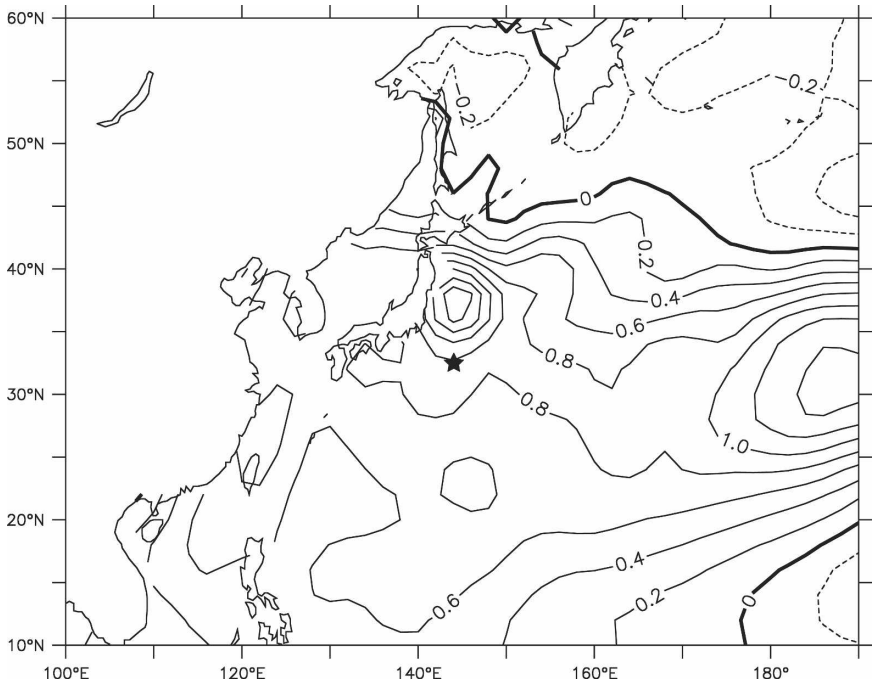


FIG. 7. Mean SST anomaly (contour interval 0.2°C) for October–March 1999–2002.

As for our analysis of the weather associated with short-term extremes in $Q_{\text{turb}}$, we created composites using a threshold of one standard deviation, in this case considering seasonal mean values of $Q_{\text{turb}}$. The same procedure was carried out for the entire record of 1950 through 2005, thereby including the prominent warm SST anomaly of 1999–2002 (not shown). In both the truncated and entire records (not shown), the patterns of anomalous SLP for the years with anomalously high (Fig. 8a) and low (Fig. 8b) $Q_{\text{turb}}$ indicate weak and statistically insignificant anomalies in pressure and pressure gradients in the vicinity of KEO. In addition, the patterns for the high and low $Q_{\text{turb}}$ composites are less mirror images of one another as compared with their counterparts regarding short-term variations in $Q_{\text{turb}}$.

The lower-tropospheric air temperatures are only slightly cooler near KEO during those seasons with strong versus weak $Q_{\text{turb}}$. Moreover, the 850-hPa temperature pattern keyed on seasonal mean flux anomalies (Fig. 8c) features an east–west oriented band of negative anomalies extending from the northern Sea of Japan to the east-northeast of KEO, while the pattern keyed on high-frequency, episodic flux events (Fig. 2d) features a southwest–northeast band of negative anomalies from off the coast of China to north of KEO. Our interpretation of these results is that the atmospheric variability is much less important in determining $Q_{\text{turb}}$ on interannual than on subseasonal (daily to weekly) time scales. The lack of much connection between $Q_{\text{turb}}$ and atmospheric variability on longer time scales essentially solidifies the findings of previous studies, namely, Kelly (2004) and Kelly and Dong (2004).

A map for the difference in SST between the strong and weak $Q_{\text{turb}}$ years (Fig. 8d) helps illustrate the importance of regional oceanic variability on interannual time scales. The key aspect of this SST difference distribution is the region of large negative (approximately $-0.8$°C) values near 40°N, 140°E. This location is directly upwind of KEO, in terms of the mean ABL flow, during both the strong and weak $Q_{\text{turb}}$ years in a composite sense, since the mean wind direction for these years is basically the same. Note also that the SST signal in this upwind or source region is greater than that in 850-hPa air temperature (Fig. 8c). The ABL over the KEO in these two sets of years therefore experiences a different degree of preconditioning from a thermodynamic perspective. In other words, there is the tendency for thermal disequilibrium between the atmosphere and ocean at KEO to be larger (smaller), and hence $Q_{\text{turb}}$ to be stronger (weaker), when the upstream $Q_{\text{turb}}$ is weaker (stronger).

A complementary perspective to the maps of Figs. 8a–d is provided by consideration of the linear correlations between interannual variations in cold season $Q_{\text{turb}}$ and local atmospheric and oceanic parameters. This analysis is restricted to simultaneous correlations: previous results on lagged relationships using a shorter record are provided by Murakami and Kawamura

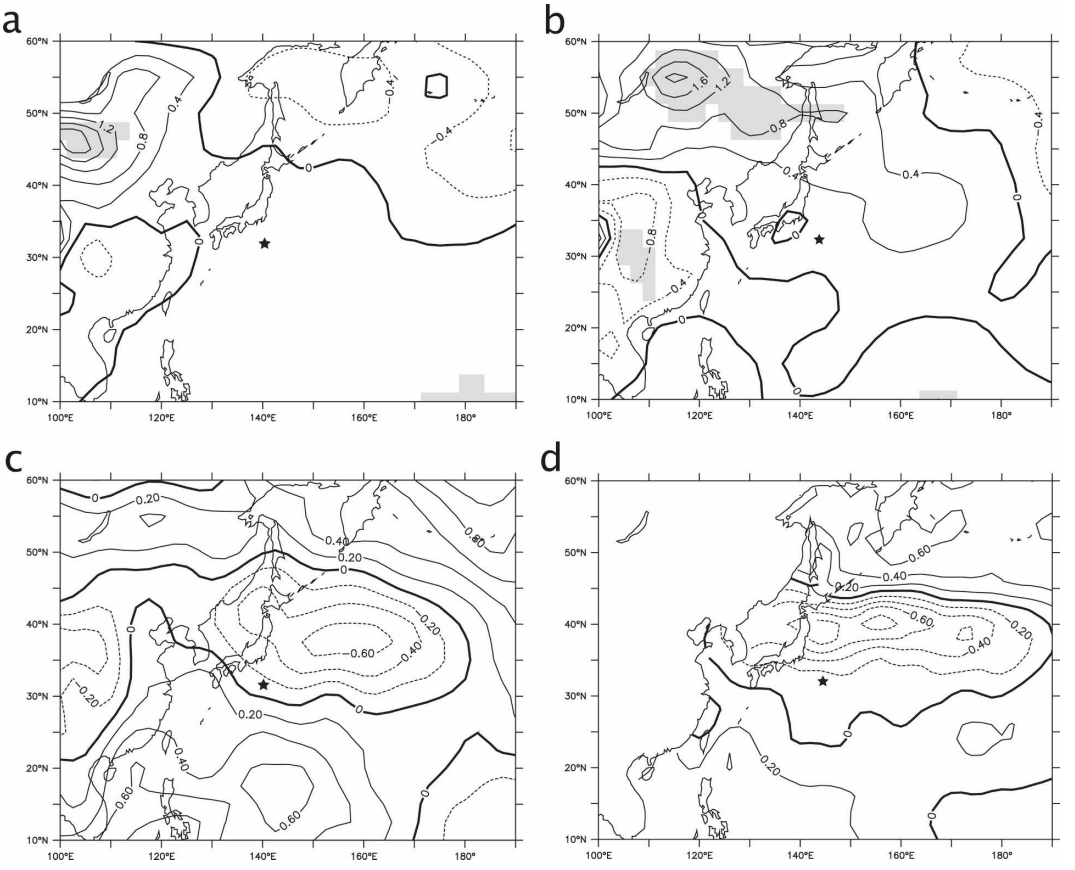


FIG. 8. Cold season (a) SLPA (contour interval 0.4 mb) with $Q_{\text{turb}}$ greater than the mean by more than 1 std dev, (b) SLPA (contour interval 0.4 mb) with $Q_{\text{turb}}$ less than the mean by more than 1 std dev, (c) difference in 850-hPa air temperature (contour interval 0.2°C) between anomalously high and low $Q_{\text{turb}}$ years, and (d) difference in SST (contour interval 0.2°C) between anomalously high and low $Q_{\text{turb}}$ years. Shading in (a) and (b) indicates where SLPA signals are statistically significant, based on the standard deviation in seasonal mean SLP from 1949 to 2005. The star indicates location of the KEO.

(2001). The magnitudes of the correlations for the entire record (including 1999–2002) are shown in the middle column of Table 3 and indicate that, of the local thermodynamic variables, it is the SST that corresponds best with the surface heat fluxes. Not only are the correlation coefficients with the NNR surface air temperature ($T_{\text{air}}$) and surface specific humidity ($q_{\text{air}}$) small, but they are of the wrong sign, in that neglecting other factors, the fluxes should be inversely related to $T_{\text{air}}$ and $q_{\text{air}}$. Note that the correlation coefficient between the fluxes and the 850-hPa temperature was also slightly positive (0.14). While this magnitude is not statistically significant, it hints that the atmosphere in the vicinity of KEO is more responding to, rather than forcing, the flux variability and that this influence of the underlying SST extends through a deep boundary layer. A relatively important role for the ocean in determining seasonal mean air–sea thermodynamic differences is also suggested by the lack of a correlation between the fluxes and the meridional wind. The latter result is in contrast with what was found on subseasonal time scales, for which the variations in the fluxes are strongly related to the meridional winds, as evidenced by the SLPA maps of Figs. 2b and 2c.

TABLE 3. Correlation coefficients involving interannual variations in mean $Q_{\text{turb}}$ ($Q_h + Q_e$) during the cold season (October–March) from NNR. Boldface entries indicate statistical significance at the 90% confidence level.

| | $r$ | $r < 1999$ |
|---|---|---|
| SST | **0.36** | −0.10 |
| $T_{\text{air}}$ | 0.14 | −0.07 |
| $q_{\text{air}}$ | 0.06 | −0.14 |
| $V_{850}$ | 0.01 | −0.09 |
| $U_*$ | **0.65** | **0.67** |
| Niño-3.4 | −0.12 | −0.02 |
| WP | 0.07 | −0.06 |
| PDO | −0.07 | −0.06 |

There is a strong, positive relationship, as might be expected, between the strength of the winds (specifically the mean friction velocity) and the fluxes. This result may seem inconsistent with the finding of only weak SLPA distributions in the vicinity of KEO during cold seasons with enhanced and suppressed $Q_{\text{turb}}$. While it is not apparent from the SLPA maps of Figs. 8a and 8b, the winds are about 4% stronger than the mean during the enhanced flux years and 7% weaker during the suppressed flux years (based on daily averages), which does contribute to the differences in $Q_{\text{turb.}}$ By way of comparison, the fluxes themselves are about 13% stronger and 16% weaker on average in the two sets of years, which implies that the difference in wind speed is not the primary cause of the difference in fluxes. In fact, the mean wind speeds may to a substantial degree represent an effect of the fluxes. As discussed by Nonaka and Xie (2003) and others, greater $Q_{\text{turb}}$, all other things equal, implies more mixing of the atmospheric surface layer and, hence, stronger surface winds.

The record at KEO prior to 1999 indicates a somewhat different relationship between the fluxes and various local parameters of the atmosphere–ocean system. Most importantly, the correlation coefficient between interannual variations in cold season $Q_{\text{turb}}$ and SST is weakly negative, implying that the fluxes are more of a cause than an effect of the SST variability (albeit to a minor and statistically insignificant extent). This is consistent with the weakly negative values for the correlation coefficients involving $T_{\text{air}}$ and $Q_{\text{air}}$, which imply a greater role for the atmosphere in driving air–sea disequilibrium. It bears emphasizing that the magnitudes of the correlation coefficients for all three parameters are quite small, which suggests not only a mix of cause and effect for each parameter, but also the importance of external influences such as horizontal advection on the seasonal mean states of both the atmosphere and ocean.

The correlations between interannual variations in $Q_{\text{turb}}$ and selected climate indices are also itemized in Table 3. The three indices considered are Niño-3.4 as a proxy for El Niño–Southern Oscillation (ENSO), the West Pacific Oscillation (WP), which is the primary atmospheric teleconnection mode in the region of interest (Wallace and Gutzler 1981), and the Pacific decadal oscillation (PDO), which constitutes the leading mode of SST variability in the North Pacific. The magnitudes of all correlation coefficients are small. Apparently, the primary modes of large-scale climate variability, or at least the ones that have been previously used to characterize this variability, have minimal projection on the regional states of the atmosphere and ocean that control the flux variability in the vicinity of KEO. For the sake of brevity, here we have considered only simultaneous relationships. Previous work has shown that oceanic conditions in the region of the Kuroshio Extension reflect a lagged response to atmospheric forcing in the central Pacific (Miller et al. 1998; Seager et al. 2001; Qiu and Chen 2005; among others). It is therefore possible that there are actually some significant linkages between the fluxes at KEO and basin-scale variability.

We now turn our attention to the warm season. The mean values of $U_*$, SST, and the fractional cloud coverage from ICOADS for the warm seasons of 1954–2005 are plotted in Fig. 9. These time series indicate less year-to-year differences in wind mixing but greater variability in SST than during the cold season. The latter result is to be expected, even though one might suppose that the variability in atmospheric forcing is greater during the cold season. The shallow depth of the oceanic mixed layer in the warm season makes the SST relatively sensitive to variations in the heat fluxes at the surface (and the base of the thermocline) during that time of year. It is interesting that the prominent recent maximum in SST at KEO during the warm season occurred about 18 months before its counterpart for the cold season (Fig. 6). The fractional cloudiness, which is a parameter related to $Q_{\text{rad}}$, rather than $Q_{\text{turb}}$, is plotted in Fig. 9 because, as discussed earlier, the net surface heating during the warm season, and its variability, is dominated by radiative effects, specifically solar heating.

The SLPA pattern for the cloudy summers (Fig. 10a) features a band of lower than normal pressure extending from East Asia out into the central Pacific between roughly 25° and 40°N. This signature suggests that a southward displaced storm track in the western Pacific tends to cause greater cloudiness near KEO, consistent with the results of Norris (2000). This SLPA pattern has both similarities and differences with that associated with the episodic heat loss in the warm season (Fig. 3b). Specifically, both maps include positive SLPA extending from the Sea of Okhotsk into the Bering Sea and negative SLPA over East Asia, but a prominent negative anomaly in SLP is located over KEO during the cloudy years (Fig. 10a) and located southwest of KEO during the episodic cooling events (Fig. 3b). Some of this difference is liable to be attributable to the selection criteria, which include consideration of $Q_{\text{turb}}$ for the episodic events, but are restricted to cloudiness in terms of the interannual variations. The SLPA pattern during relatively clear warm seasons (Fig. 10b) indicates relatively low pressure over East Asia and high

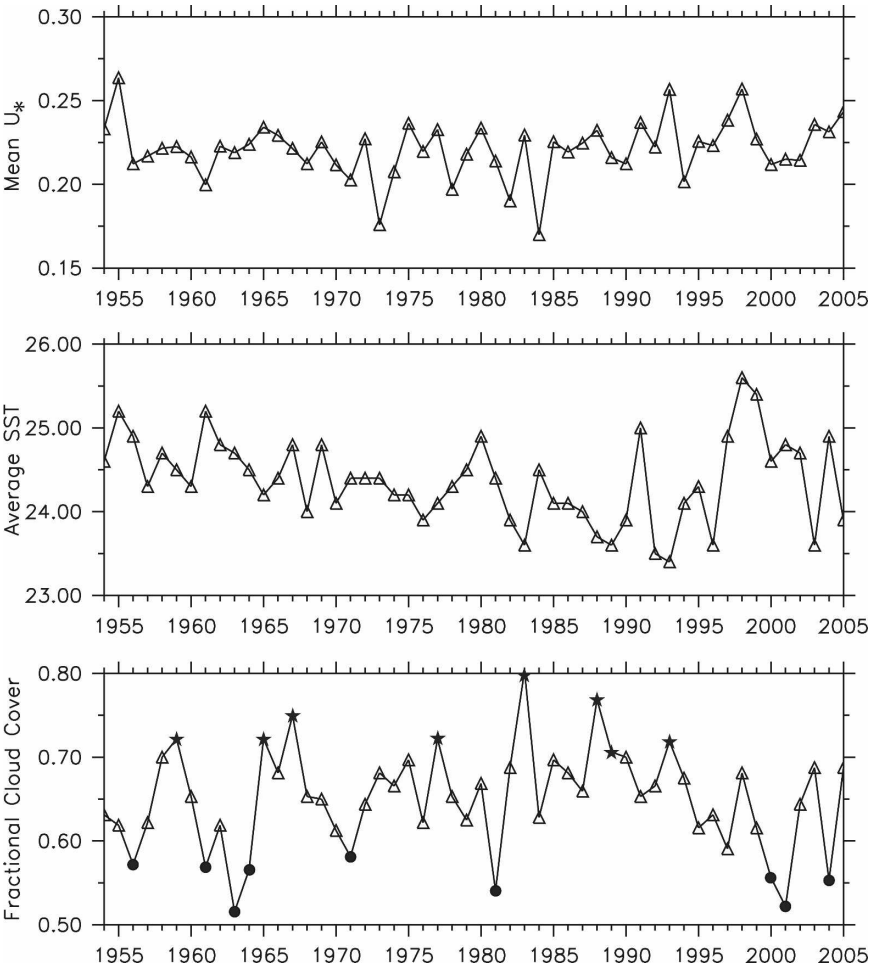


FIG. 9. Mean warm season (top) $U_*$ (m s$^{-1}$), (middle) SST (°C) from NNR, and (bottom) fractional cloud coverage from ICOADS at KEO. The years included in the cloudy and clear composites are indicated with stars and closed circles, respectively.

pressure near the date line north of 40°N. The sense of this pattern resembles that for the periods of episodic heating (Fig. 3c) over the western Pacific in the region of KEO. It also resembles the pattern of 850-hPa streamfunction anomalies shown by Ueda and Kawamura (2004) for the summers of 1999–2001, which featured warm SSTs and enhances insolation in the region of the Kuroshio Extension. Ueda and Kawamura (2004) suggest that this situation may be associated with a stationary Rossby wave excited by enhanced convective heating northwest of the Philippines. A band of cooler lower-tropospheric temperatures extends from East Asia into the central North Pacific in relatively cloudy versus clear warm seasons at KEO (Fig. 10c). This supports the idea that clouds in the region of KEO are enhanced during periods when the lower-tropospheric baroclinic zone and storm track is displaced south of its usual latitude.

A map of the difference in SST between the cloudy and clear warm seasons (Fig. 10d) features a band of negative values along 35°N from the Sea of Japan extending eastward past the date line. This band is centered where the meridional gradient in 850-hPa air temperature is enhanced (Fig. 10c). The relatively cool SSTs in this band reflect the reduction in solar heating of the ocean during cloudy conditions, but there may also be some positive air–sea interaction feedbacks. Since the mean ABL flow in the region of KEO is from the south, the SST pattern of Fig. 10d indicates that this flow is over increasingly cooler SSTs to a greater extent during cloudy than cool years. This has the effect of stabilizing the ABL in the former relative to the latter years, which may cause the preferential development of stratus cloud decks of high fractional coverage (Norris and Leovy 1994).

Correlation coefficients between the seasonal mean

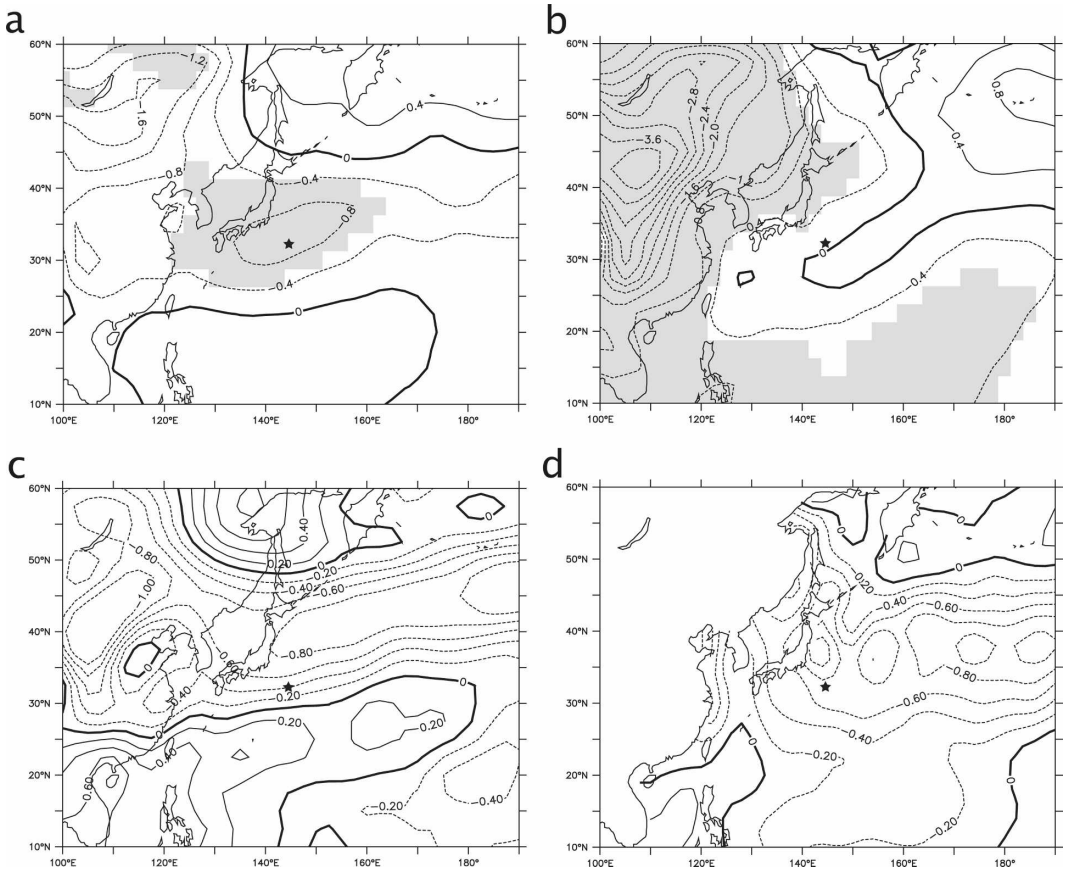


FIG. 10. Warm season (a) SLPA (contour interval 0.4 mb) with cloudiness greater than the mean by more than 1 std dev, (b) SLPA (contour interval 0.4 mb) with cloudiness less than the mean by more than 1 std dev, (c) difference in 850-hPa air temperature between anomalously high and low cloudiness years (contour interval 0.2°C), and (d) difference in SST (contour interval 0.2°C), between anomalously high and low cloudiness years. Shading in (a) and (b) indicates where SLPA signals are statistically significant, based on the standard deviation in seasonal mean SLP from 1954 through 2005. The star indicates location of the KEO.

variations in cloud fraction at KEO from ICOADS and various measures of the local parameters, and climate indices, are itemized in Table 4. Relatively cloudy conditions at KEO tend to be accompanied by cool SSTs, as would be expected based on the SST difference map of Fig. 10d. Cloudy versus clear seasons also include a weak tendency toward stronger winds, but a negligible signal in 850-hPa specific humidity ($q_{850}$).

As for $Q_{\text{turb}}$ during the cold season, we have investigated the simultaneous correlations between interannual variations in seasonal mean cloudiness and climate indices during the warm season. It is plausible that there would be linkages between the East Asian summer monsoon (EASM), in particular, rainfall in Japan accompanying the baiu front, and the weather patterns associated with cloudiness anomalies at KEO. In an overall sense, the SLP and 850-hPa air temperature anomalies favoring clouds at KEO, in particular anomalous troughing extending from China across Japan into the west Pacific accompanied by enhanced low-level baroclinity, imply a relatively strong baiu front and, presumably, enhanced rainfall. It is not surprising that such a connection would exist in that interannual variations in the western flank of the subtropical

TABLE 4. Correlation coefficients involving interannual variations in mean fractional cloudiness during the warm season (May–August) from ICOADS. Boldface entries indicate statistical significance at the 90% confidence level.

| | $r$ |
|---|---|
| SST | **−0.47** |
| $q_{850}$ | −0.04 |
| $U_*$ | **0.20** |
| WNPSMI | **−0.28** |
| Niño-3.4 | 0.04 |
| WP | −0.18 |
| PDO | **0.33** |

high over the Pacific have been found to be related to variations in the EASM (as reviewed by Yihui and Chan 2005) and should relate to cloudiness and, ultimately, fluctuations in seasonal heating in the region of KEO. As a means of pursuing this issue, we have correlated the interannual variations in cloudiness at KEO with the index for the western North Pacific summer monsoon (WNPSMI) of Wang et al. (2001). They argued that a strong (weak) value of the WNPSMI should tend to be associated with a weak (strong) baiu frontal zone and, correspondingly, suppressed (enhanced) cloudiness extending eastward from Japan, leading to relatively warm (cool) SSTs. The correlation coefficient between the cloudiness at KEO and WNPSMI ($r$ aproximately $-0.28$; Table 4) is consistent with this reasoning, albeit to a moderate degree. The magnitude of this correlation is greater than that for the WP (which is statistically insignificant). It is interesting that the cloudiness is essentially uncorrelated with ENSO in terms of the Niño-3.4 index, but is significantly correlated with the PDO. It turns out that the SLPA pattern for the relatively clear warm seasons at the KEO location (Fig. 10b) resembles the mirror image of the SLP distribution over the western North Pacific found through regression of the May–August mean of the PDO. Our analysis is unable to sort out the mechanisms responsible for this relationship. In general, our results suggest that the climate system, at least as encapsulated by commonly used indices, relates more to mean cloudiness in the warm season than to $Q_{\text{turb}}$ in the cold season in the vicinity of KEO.

## 5. Concluding remarks

The surface heat fluxes of the Kuroshio Extension, and its attendant recirculation gyre, form an important link in the North Pacific branch of the global heat cycle. These fluxes undergo substantial fluctuations on time scales of days to decades, reflecting a response to both atmospheric and oceanic influences. The present study has exploited the, unprecedented, direct measures of these fluxes from the KEO air–sea flux surface mooring to describe how they relate to regional weather patterns.

Some interesting comparisons can be made between the weather patterns associated with episodic high-frequency flux events and the counterpart patterns associated with interannual flux variations at the KEO location. We recognize that each set of weather patterns is subject to some ambiguity. The set of episodic events is drawn from the period of the deployment of the KEO surface buoy between June 2004 and November 2005 and, hence, may not be fully representative of long-term conditions and relationships. The set of anomalous years is based on $Q_{\text{turb}}$ from the NNR to identify the cold seasons with anomalous net heat fluxes, and cloud coverage observations from ICOADS to identify the warm seasons with anomalous shortwave irradiance and hence net heating. Both the NNR and ICOADS datasets include errors and uncertainties. In spite of these caveats, we believe some generalizations can be based on the results presented above.

First of all, our analysis demonstrates that the weather patterns associated with high-frequency (daily to weekly) fluctuations in the net surface heat fluxes at KEO vary seasonally. During the cold season, enhanced upward fluxes and strong wind mixing, hence ocean cooling, tend to occur in anomalous northerly to northwesterly flow in association with cold air outbreaks. The concomitant modification of the ABL has been the subject of extensive study (Ninomiya 1975; Tokinaga et al. 2006; among others). While our results are not new in this respect for the cold season, they do represent an interesting contrast with those for the warm season. Anomalous cooling during the warm season at KEO tended to happen in two ways. In 2004, these events included both strong winds and hence a seasonally large positive (upward) $Q_{\text{turb}}$ component to the fluxes, and greater cloudiness and hence reduced solar heating. This appears to have been at least in part due to enhanced tropical cyclone activity; a record number of 10 named storms made landfall in Japan in 2004 (Camargo 2005). In 2005, anomalous cooling events tended to be associated with enhanced cloudiness in association with the passage of weak cyclonic disturbances of extratropical origin. While the synoptic activity varies from year to year, this variability is likely to be accompanied more by changes in the overall number and perhaps strength of individual events, rather than major changes in the nature of their associated weather patterns. Moreover, our analysis is based on the high-frequency perturbations from the mean during the KEO record rather than the climatological mean, which reduces the sensitivity of our results to the background state during the period of KEO deployment. In addition, the SLPA patterns during periods of anomalous warming were qualitatively opposite to those during periods of anomalous cooling, at least in the region of KEO. This consistency between the composite-based maps and our finding that the magnitudes of their prominent anomalies were substantial, as compared with their standard errors, suggest that our results are robust.

The degree to which the regional atmospheric structures accompanying interannual fluctuations in the fluxes resemble their high-frequency counterparts dif-

fers by season. For the cold season, the composite SLPA and 850-hPa air temperature anomalies based on seasonal mean fluxes were relatively weak in amplitude and of different patterns than those keyed on the high-frequency flux events. The 850-hPa air temperature difference map for the two cases is telling. The magnitude of this anomaly at KEO for the interannual case (Fig. 8c) is ~0.2°C or roughly 3% of that for the subseasonal case (Fig. 2d). This ratio is about five times smaller than the ratio between the standard deviation in $Q_{\text{turb}}$ in the two cases, implying that lower-tropospheric thermodynamic anomalies exert much less control on the heat fluxes on interannual than short time scales. This finding is consistent with the correlation coefficients between interannual variations in the fluxes and basic-state variables (Table 3), which were small and of inconsistent sign depending on the time span of the record considered.

The warm season represents a different story. During this time of year, the characteristic patterns of SLPA for periods of enhanced (suppressed) cloudiness on interannual time scales (Figs. 9a and 9b) more resemble those for periods of anomalous cooling (heating) on subseasonal time scales (Figs. 3b and 3c). As discussed in section 3a, anomalous cooling on subseasonal time scales during the KEO deployment tended to be associated with either cyclones of tropical origin (especially during the very active season of 2004) or cyclonic disturbances of extratropical origin, with the latter type of events having a particularly important impact on cloudiness. Because our interannual analysis is keyed on cloudiness, it will naturally reflect the weather patterns accompanying variations in extratropical cyclonic activity. The correspondence between the anomalous circulations associated with variations in net heating/cloudiness in summer suggests that the atmosphere plays a more consistent role in determining seasonal variations in the net heating in the warm season than in the cold season. On this topic, the interannual variations in cloudiness in the vicinity of the KEO are also significantly correlated ($r$ approximately $-0.47$) with the local SST (Table 4). This relationship is consistent not just with more clouds reducing $Q_{\text{sw}}$ and ultimately SST, but also the idea that positive (negative) SST anomalies serve to inhibit (promote) marine stratiform cloudiness (Norris and Leovy 1994). Our results, using a different method, essentially represent a local expression of the relationships found among clouds, SST, and SLP for the central and western North Pacific reported by Norris et al. (1998).

The objective of this study has been to better understand how the net surface heat fluxes in the vicinity relate to regional weather patterns. This work has been motivated, not just by the opportunity provided by the high-quality observations from KEO, but also because the surface fluxes at this location are so large and undergo such a strong seasonal cycle. The focus here has been on simultaneous relationships; previous studies indicate that the air–sea interactions of the region are sensitive to lagged and remote effects, but these are outside the scope of the present study. The intent of our future research is to build upon studies such as Nakamura et al. (2004) on the linkages between the ocean and atmosphere in the western North Pacific. In particular, we plan to examine the consequences of heat flux variations at the KEO, specifically for the upper ocean through a heat budget analysis and for the atmosphere through sensitivity experiments using a numerical weather prediction model.

*Acknowledgments.* The KEO time series reference site is sponsored by the National Oceanic and Atmospheric Administration (NOAA)/Office of Climate Observations (OCO). Support for N. A. Bond was provided by the CLIVAR Element of the NOAA Climate and Global Change Program (GC 06-334). This publication is funded by the Joint Institute for the Study of the Atmosphere and Ocean (JISAO) under NOAA Cooperative Agreement NA17RJ1232, Contribution 1368.

## REFERENCES

Bond, N. A., J. E. Overland, M. Spillane, and P. Stabeno, 2003: Recent shifts in the state of the North Pacific. *Geophys. Res. Lett.,* **30,** 2183, doi:10.1029/2003GL018597.

Camargo, S. J., 2005: Western North Pacific typhoon season. *Bull. Amer. Meteor. Soc.,* **86** (6), S29–S32.

Cronin, M. F., N. A. Bond, C. W. Fairall, and R. A. Weller, 2006a: Surface cloud forcing in the east Pacific stratus deck/cold tongue/ITCZ complex. *J. Climate,* **19,** 392–409.

——, C. W. Fairall, and M. J. McPhaden, 2006b: An assessment of buoy-derived and numerical weather prediction surface heat fluxes in the tropical Pacific. *J. Geophys. Res.,* **111,** C06038, doi:10.1029/2005JC003324.

Fairall, C. W., E. F. Bradley, J. E. Hare, A. A. Grachev, and J. B. Edson, 2003: Bulk parameterization of air–sea fluxes: Updates and verification for the COARE algorithm. *J. Climate,* **16,** 571–591.

Josey, S. A., E. C. Kent, and P. K. Taylor, 1998: The Southampton Oceanography Centre (SOC) Ocean–Atmosphere Heat, Momentum and Freshwater Atlas. SOC Rep. 6, Southampton Oceanography Centre, 30 pp.

Kalnay, E., and Coauthors, 1996: The NCEP/NCAR 40-Year Reanalysis Project. *Bull. Amer. Meteor. Soc.,* **77,** 437–471.

Kelly, K. A., 2004: The relationship between oceanic heat transport and surface fluxes in the western North Pacific: 1970–2000. *J. Climate,* **17,** 573–588.

——, and S. F. Dong, 2004: The relationship between western boundary current heat transport and storage to midlatitude

ocean–atmosphere interaction. *Earth's Climate: The Ocean–Atmosphere Interaction, Geophys. Monogr.,* Vol. 147, Amer. Geophys. Union, 347–363.

Kistler, R., and Coauthors, 2001: The NCEP–NCAR 50-Year Reanalysis: Monthly means CD-ROM and documentation. *Bull. Amer. Meteor. Soc.,* **82,** 247–267.

Kubota, M., N. Iwabe, M. F. Cronin, and H. Tomita, 2008: Surface heat fluxes from the NCEP/NCAR and NCEP/DOE reanalyses at the KEO buoy site. *J. Geophys. Res.,* **113,** C02009, doi:10.1029/2007JC004338.

Ladd, C., and N. A. Bond, 2002: Evaluation of the NCEP/NCAR reanalysis in the NE Pacific and the Bering Sea. *J. Geophys. Res.,* **107,** 3158, doi:10.1029/2001JC001157.

Lenschow, D. H., and E. M. Agee, 1976: Preliminary results from the Air Mass Transformation Experiment (AMTEX). *Bull. Amer. Meteor. Soc.,* **57,** 1346–1355.

Miller, A. J., D. R. Cayan, and W. B. White, 1998: A westward-intensified decadal change in the North Pacific thermocline and gyre-scale circulation. *J. Climate,* **11,** 3112–3127.

Minobe, S., 2002: Interannual to interdecadal changes in the Bering Sea and concurrent 1998/99 changes over the North Pacific. *Prog. Oceanogr.,* **55,** 45–64.

Moore, G. W. K., and I. A. Renfrew, 2002: An assessment of the surface turbulent heat fluxes from the NCEP–NCAR reanalysis over the western boundary currents. *J. Climate,* **15,** 2020–2037.

Murakami, H., and H. Kawamura, 2001: Relations between sea surface temperature and air–sea heat flux at periods from 1 day to 1 year observed at ocean buoy stations around Japan. *J. Oceanogr.,* **57,** 565–580.

Nakamura, H., T. Sampe, Y. Tanimoto, and A. Shimpo, 2004: Observed associations among storm tracks, jet streams, and midlatitude oceanic fronts. *Earth's Climate: The Ocean–Atmosphere Interaction, Geophys. Monogr.,* Vol. 147, Amer. Geophys. Union, 329–345.

Ninomiya, K., 1975: Large-scale aspects of air-mass transformation over the East China Sea during AMTEX '74. *J. Meteor. Soc. Japan,* **53,** 285–303.

——, and H. Mizuno, 1985: Anomalously cold spell in summer over northeastern Japan caused by northeasterly wind from polar maritime air mass. Part I. EOF analysis of temperature variation in relation to the large-scale situation causing the cold summer. *J. Meteor. Soc. Japan,* **63,** 845–857.

Nonaka, M., and S.-P. Xie, 2003: Covariations of sea surface temperature and wind over the Kuroshio and its extension: Evidence for atmosphere–ocean feedback. *J. Climate,* **16,** 1404–1413.

Norris, J. R., 2000: Interannual and interdecadal variability in the storm track, cloudiness, and sea surface temperature over the summertime North Pacific. *J. Climate,* **13,** 422–430.

——, and C. B. Leovy, 1994: Interannual variability in stratiform cloudiness and sea surface temperature. *J. Climate,* **7,** 1915–1925.

——, Y. Zhang, and J. M. Wallace, 1998: Role of low clouds in summertime atmosphere–ocean interactions over the North Pacific. *J. Climate,* **11,** 2482–2490.

Qiu, B., and S. Chen, 2005: Variability of the Kuroshio Extension jet, recirculation gyre, and mesoscale eddies on decadal time scales. *J. Phys. Oceanogr.,* **35,** 2090–2103.

——, ——, and P. Hacker, 2004: Synoptic-scale air–sea flux forcing in the western North Pacific: Observations and their impact on SST and the mixed layer. *J. Phys. Oceanogr.,* **34,** 2148–2159.

Quan, X., M. Hoerling, J. Whitaker, G. Bates, and T. Xu, 2006: Diagnosing sources of U.S. seasonal forecast skill. *J. Climate,* **19,** 3279–3293.

Renfrew, I. A., G. W. K. Moore, P. S. Guest, and K. Bumke, 2002: A comparison of surface layer and surface turbulent flux observations over the Labrador Sea with ECMWF analyses and NCEP reanalyses. *J. Phys. Oceanogr.,* **32,** 383–400.

Seager, R., Y. Kushnir, N. H. Naik, M. A. Cane, and J. Miller, 2001: Wind-driven shifts in the latitude of the Kuroshio–Oyashio extension and generation of SST anomalies on decadal timescales. *J. Climate,* **14,** 4249–4265.

Tanimoto, Y., H. Nakamura, T. Kagimoto, and S. Yamane, 2003: An active role of extratropical sea surface temperature anomalies in determining anomalous turbulent heat flux. *J. Geophys. Res.,* **108,** 3304, doi:10.1029/2002JC001750.

Tokinaga, H., and Coauthors, 2006: Atmospheric sounding over the winter Kuroshio Extension: Effect of surface stability on atmospheric boundary layer structure. *Geophys. Res. Lett.,* **33,** L04703, doi:10.1029/2005GL025102.

Tomita, H., and M. Kubota, 2005: Increase in turbulent heat flux during the 1990s over the Kuroshio/Oyashio extension region. *Geophys. Res. Lett.,* **32,** L09705, doi:10.1029/2004GL022075.

Trenberth, K. E., and J. M. Caron, 2001: Estimates of meridional atmosphere and ocean heat transports. *J. Climate,* **14,** 3433–3443.

Ueda, H., and R. Kawamura, 2004: Summertime anomalous warming over the midlatitude western North Pacific and its relationships to the modulation of the Asian Monsoon. *Int. J. Climatol.,* **24,** 1109–1120.

Wallace, J. M., and D. S. Gutzler, 1981: Teleconnections in the geopotential height field during the Northern Hemisphere winter. *Mon. Wea. Rev.,* **109,** 784–812.

Wang, B., R. Wu, and K.-M. Lau, 2001: Interannual variability of the Asian summer monsoon: Contrasts between the Indian and western North Pacific–East Asian monsoons. *J. Climate,* **14,** 4073–4090.

Yihui, D., and J. C. L. Chan, 2005: The East Asian summer monsoon: An overview. *Meteor. Atmos. Phys.,* **89,** 117–142.